Hierarchy of signaling thresholds downstream of the T cell receptor and the Tec kinase ITK

Michael P. Gallagher[a], James M. Conley[b], Pranitha Vangala[c], Manuel Garber[c], Andrea Reboldi[a], and Leslie J. Berg[a,b,1]

[a]Department of Pathology, University of Massachusetts Medical School, Worcester, MA 01605; [b]Department of Immunology and Microbiology, University of Colorado Anschutz School of Medicine, Aurora, CO 80045; and [c]Program in Bioinformatics and Integrative Biology, University of Massachusetts Medical School, Worcester, MA 01605

Edited by Anjana Rao, La Jolla Institute for Immunology, La Jolla, CA, and approved June 9, 2021 (received for review December 17, 2020)

The strength of peptide:MHC interactions with the T cell receptor (TCR) is correlated with the time to first cell division, the relative scale of the effector cell response, and the graded expression of activation-associated proteins like IRF4. To regulate T cell activation programming, the TCR and the TCR proximal interleukin-2–inducible T cell kinase (ITK) simultaneously trigger many biochemically separate signaling cascades. T cells lacking ITK exhibit selective impairments in effector T cell responses after activation, but under the strongest signaling conditions, ITK activity is dispensable. To gain insight into whether TCR signal strength and ITK activity tune observed graded gene expression through the unequal activation of distinct signaling pathways, we examined Erk1/2 phosphorylation or nuclear factor of activated T cells (NFAT) and nuclear factor (NF)-κB translocation in naïve OT-I CD8$^+$ cell nuclei. We observed the consistent digital activation of NFAT1 and Erk1/2, but NF-κB displayed dynamic, graded activation in response to variation in TCR signal strength, tunable by treatment with an ITK inhibitor. Inhibitor-treated cells showed the dampened induction of AP-1 factors *Fos* and *Fosb*, NF-κB response gene transcripts, and survival factor *Il2* transcripts. ATAC sequencing analysis also revealed that genomic regions most sensitive to ITK inhibition were enriched for NF-κB and AP-1 motifs. Specific inhibition of NF-κB during peptide stimulation tuned the expression of early gene products like c-Fos. Together, these data indicate a key role for ITK in orchestrating the optimal activation of separate TCR downstream pathways, specifically aiding NF-κB activation. More broadly, we revealed a mechanism by which variations in TCR signal strength can produce patterns of graded gene expression in activated T cells.

T cell receptor signaling | T cell activation | ITK | NFAT | NF-κB

After T cell receptor (TCR) triggering, a single naïve CD8$^+$ T cell has the potential to expand into millions of daughter effector cells, which use cytolytic factors to eradicate virus-infected cells. The strength of the interaction between the TCR and cognate peptide:MHC molecules on antigen-presenting cells (APCs) controls the rapidity, the response, and the ultimate scale of the effector pool. Stronger-affinity TCR interactions lead to prolonged periods of proliferation and longer times of engagement with APCs, thereby producing larger pools of CD8$^+$ effector T cells (1–3).

TCR triggering and proximal signaling events exhibit noisy, switch-like behavior. The kinetic proofreading model of TCR signal initiation posits that ligand discrimination is determined by the accumulation of rate-limiting signaling intermediates, which elicit the committed activation of transcription factors. Strong peptide:MHC ligands bind frequently with the TCR and overcome these rate-limiting steps, while weak ligands bind less frequently and are less likely to accumulate signaling intermediates (4–6). Individual downstream transcription factors pathways also display digital signaling behaviors. TCR-mediated, store-operated calcium (Ca^{2+}) entry (SOCE) and the subsequent nuclear factor of activated T cells (NFAT) activation display probabilistic, digital triggering corresponding to the dose of peptide:MHC (7–10). We recently demonstrated that NFAT1 nuclear translocation in response to TCR stimulation is a digital process, as ovalbumin (OVA) peptide concentration modulates the frequency of responder cells within a naïve, clonal OT-I T cell population, without affecting the amount of NFAT1 protein measured in individual, responding cell nuclei (10). Similar bimodal behavior is described for extracellular signal-regulated kinase (Erk) activation, as OVA peptide dose carefully tunes the number of digitally activated Erk responders in a pool of naïve OT-I cells (11, 12). The behavior of these pathways is enforced through feedback mechanisms (Erk) and the rapid regulation of phosphorylation states (NFAT) (8, 12). Nuclear factor (NF)–κB signaling in T cells has also been observed to behave digitally under some conditions (13). Following TCR engagement, these separate pathways activate in parallel. However, careful observation of the simultaneous and relative behavior of each pathway in T cells in response to peptide stimulation is lacking (14).

Peptide concentration and avidity contribute to the probability of digital TCR triggering in individual cells, but at the same time, these same variables tune the graded expression of important, effector-associated factors, notably interferon regulatory factor (IRF)4 and CD25 (10, 12, 15, 16). This disconnect prompted us to question how graded gene expression patterns emerge from digital signaling events. Interleukin-2–inducible T cell kinase (ITK) is a critical component for the optimal activation of phospholipase-C-gamma-1 (PLC-γ1), the enzyme that cleaves the membrane-embedded phosphatidylinositol bisphosphate into equimolar amounts of two second signaling messengers: inositol triphosphate (IP_3) and diacylglycerol (DAG). IP_3 and DAG are

Significance

In order to help fight off pathogens and malignancies, CD8$^+$ T lymphocytes send signals from the T cell receptor (TCR) through multiple transcription factor pathways. The strength of the TCR signal is modulated in part by the Tec kinase ITK, whose activity helps create graded amounts of T cell activation genes. We report that some signaling pathways rely more heavily on ITK support for robust activation. During suboptimal signaling conditions, we measured the reduced amount of NF-κB activation and early gene induction within digital NFAT- and Erk1/2-activated cells. Our work highlights the importance of signal strength in activating T cells and uncovers details about the supplemental role of ITK in proximal TCR signaling.

Author contributions: M.P.G., J.M.C., P.V., M.G., and L.J.B. designed research; M.P.G. and J.M.C. performed research; M.P.G., J.M.C., P.V., M.G., A.R., and L.J.B. analyzed data; and M.P.G. and L.J.B. wrote the paper.

The authors declare no competing interest.

This article is a PNAS Direct Submission.

[1]To whom correspondence may be addressed. Email: leslie.berg@cuanschutz.edu.

This article contains supporting information online at https://www.pnas.org/lookup/suppl/doi:10.1073/pnas.2025825118/-/DCSupplemental.

Published August 27, 2021.

responsible for the robust activation of downstream TCR signaling pathways, including NFAT, Erk, and nuclear factor (NF)-κB (17, 18). Although TCR signaling is not completely abolished in the absence of ITK, T cells from *Itk*$^{-/-}$ mice show inefficient, intracellular Ca^{2+} flux and have notable defects in Erk phosphorylation (p-Erk) (19–22). Stimulation of naïve *Itk*$^{-/-}$ OT-I cells or treatment with a small molecule ITK inhibitor reduced the induction of IRF4 (15), indicating that ITK may not regulate gene expression in an all-or-none fashion but rather act as a rheostat to carefully tune TCR signaling.

To determine whether ITK differentially regulates digital TCR responses to tune-graded gene expression, we measured simultaneous NFAT1, NF-κB, and Erk activation in single naïve OT-I T cells stimulated with peptides of variable affinity with or without the use of an inhibitor of ITK (and resting lymphocyte kinase, RLK). We found that NFAT1 and Erk activation consistently showed digital responses, even in weakly stimulated cells; however, each pathway had a different sensitivity to ITK/RLK inhibition. Importantly, NF-κB activation occurred incrementally; cells that digitally triggered NFAT1 had graded amounts of NF-κB activation that scaled with peptide affinity and was sensitive to ITK/RLK inhibition. We also measured the immediate transcriptional response following different TCR signaling conditions. These studies revealed that the expression of NF-κB gene targets and the induction of transcripts encoding AP-1 factors were most sensitive to ITK/RLK inhibition. Regions of dynamic DNA accessibility most sensitive to ITK/RLK inhibition were also enriched for NF-κB and AP-1 binding motifs. Inhibition of NF-κB activation in stimulated OT-I cells altered TCR-induced gene expression in a pattern that mirrored the effects ITK/RLK inhibition. Together, these data underscore a role for ITK as an amplifier of TCR signaling and demonstrate a critical role for ITK in tuning NF-κB signaling in digitally activated naïve CD8$^+$ T cells.

Results

Signaling pathway activation after TCR engagement has largely been described as digital, in which TCR triggering is determined by a threshold for activation. When this threshold is exceeded, downstream responses of NFAT, NF-κB, and MAPK then "switch on" together (9, 12, 13). The probability that a TCR stimulus will digitally activate an individual naïve T cell within a stimulated, clonal population is measured by examining the fraction of cells that up-regulate the cell surface marker CD69 (11, 12, 16, 18). Cells experiencing weakened TCR stimulation may sufficiently switch on digital CD69 expression but fail to maximally up-regulate important, effector-associated factors like IRF4 (16). Additionally, CD69 expression does not explicitly guarantee that a T cell will be sufficiently stimulated to commit to clonal expansion and effector programming (23, 24). Thus, there are signaling behaviors underlying digital triggering that generate divergent gene expression programs and ultimately contribute to a naïve T cell's fate. We hypothesized that the activity of the TCR proximal tyrosine kinase ITK is sensitive to the variable amount of TCR stimulation, in order to tune the intensity of downstream signaling pathways, and the graded transcription of a subset of genes induced in digitally activated cells.

ITK/RLK Inhibition Differentially Dampens Gene Expression in Activating OT-I Cells. To test whether tunable ITK activity modulates TCR signaling during activation, we measured gene expression in CD8$^+$ T cells treated with a covalent small molecule inhibitor (PRN694) (25). PRN694 is a compound highly selective for the active site of both ITK and RLK; RLK is a kinase coexpressed in naïve T cells structurally similar to ITK without clear function in TCR signaling (26). Thymically derived *Itk*$^{-/-}$ cells do not develop normally (22). Thus, PRN694 allows for the titrated control of ITK/RLK activity in naïve wild-type (WT) OT-I cells and assures both untreated and treated naïve cell transcriptional states are similar before stimulation. To regulate TCR signaling via differential ligand stimulation, we utilized OVA peptide plus altered peptide ligands, in which graded peptide potency is achieved using residue substitutions within the native "SIIN**F**EKL" OVA peptide (N4) (2). After stimulation with weaker affinity "SII**T**FEKL" (T4) altered OVA peptide, a similar number of ITK/RLK inhibitor-treated and -untreated OT-I CD8$^+$ T cells up-regulated CD69, but inhibitor-treated cells exhibited dampened expression of IRF4 (Fig. 1*A*). This confirmed that the ITK/RLK inhibitor has a differential effect on specific, activation-induced genes, similar to studies examining *Itk*$^{-/-}$ OT-I cells (16). Inhibitor-treated, T4-stimulated cells also displayed less proliferative potential measured at 48 h, with a large percentage of cells remaining undivided (Fig. 2*B*). Thus, under these conditions, ITK/RLK activity is dispensable for the switch-like induction of the activation marker CD69 but critical in tuning the intensity of other important genes that govern T cell activation programming and cell division.

NF-κB Activation Is Tunable in Digitally Activated Naïve OT-I Cells. Pathways downstream of the TCR, critical for robust T cell activation, are highly dependent on the activation of NFAT, NF-κB, and AP-1 transcription factor families (18, 27, 28). We hypothesized that each pathway may have different sensitivity to varied amounts of upstream TCR stimulation or ITK activity and that differential signaling patterns could contribute to the graded expression of activation-associated factors. Naïve cells have NFAT and NF-κB factors sequestered in the cytoplasm, such that TCR engagement induces their rapid translocation to the nucleus (28, 29). To measure activation of NFAT and NF-κB in single cells, we performed flow cytometry with stimulated OT-I nuclei, as described previously (10). This technique allowed us to quantify both the proportion of OT-I cells responding to stimulation as well as the relative abundance of each factor within individual, stimulated nuclei.

After strong peptide:MHC stimulation, we observed that NFAT1 and NF-κB (p65) quickly translocated to the nucleus (Fig. 1*C*). Erk-MAPK signaling was also rapidly activated in nearly all stimulated OT-I cells, as measured by conventional phospho-Erk1/2 (p-Erk) fluorescence. These rapid responses confirmed previously reported "switch-like" signaling behavior after TCR engagement (7, 10–13). However, in response to weaker peptide stimulation, differences between pathways became more evident. Stimulation with T4 (altered OVA peptide) produced a slower accumulation of the OT-I population that exhibited nuclear NFAT1 and p-Erk than stimulation with the high-avidity OVA peptide, N4. Stimulation with T4 reduced the maximum proportion of NFAT1 positive nuclei by 2 h of stimulation from ~90% (with N4) to 75% (T4) (Fig. 1 *D–F*). Importantly, we observed minimal differences in NFAT1 or p-Erk median fluorescence intensity (MFI) within responding nuclei or cells, indicating that these pathways remained digitally triggered, even under weaker signaling conditions (Fig. 1*D*). In contrast, TCR stimulation with T4 peptide failed to optimally activate NF-κB, as evident by both the reduced number of responder cells and by a lower intensity of NF-κB fluorescence in single OT-I nuclei (Fig. 1*D*). Intermediate intensity of nuclear NF-κB (p65) suggested that TCR control of the NF-κB pathway did not behave digitally, as was observed for NFAT1 and p-Erk1/2 activation. Furthermore, compared with chemical activation with PMA and ionomycin, peptide:MHC-stimulated OT-I cells activated NF-κB with suboptimal intensity, while NFAT1 activation in the same cell nuclei was similar between the two stimulation conditions (Fig. 1*E*). These findings demonstrated that, under more physiological peptide stimulation conditions, NF-κB is more tunable to the level of TCR engagement than NFAT1 and p-Erk and revealed a dynamic range of activation states within a population of stimulated T cells.

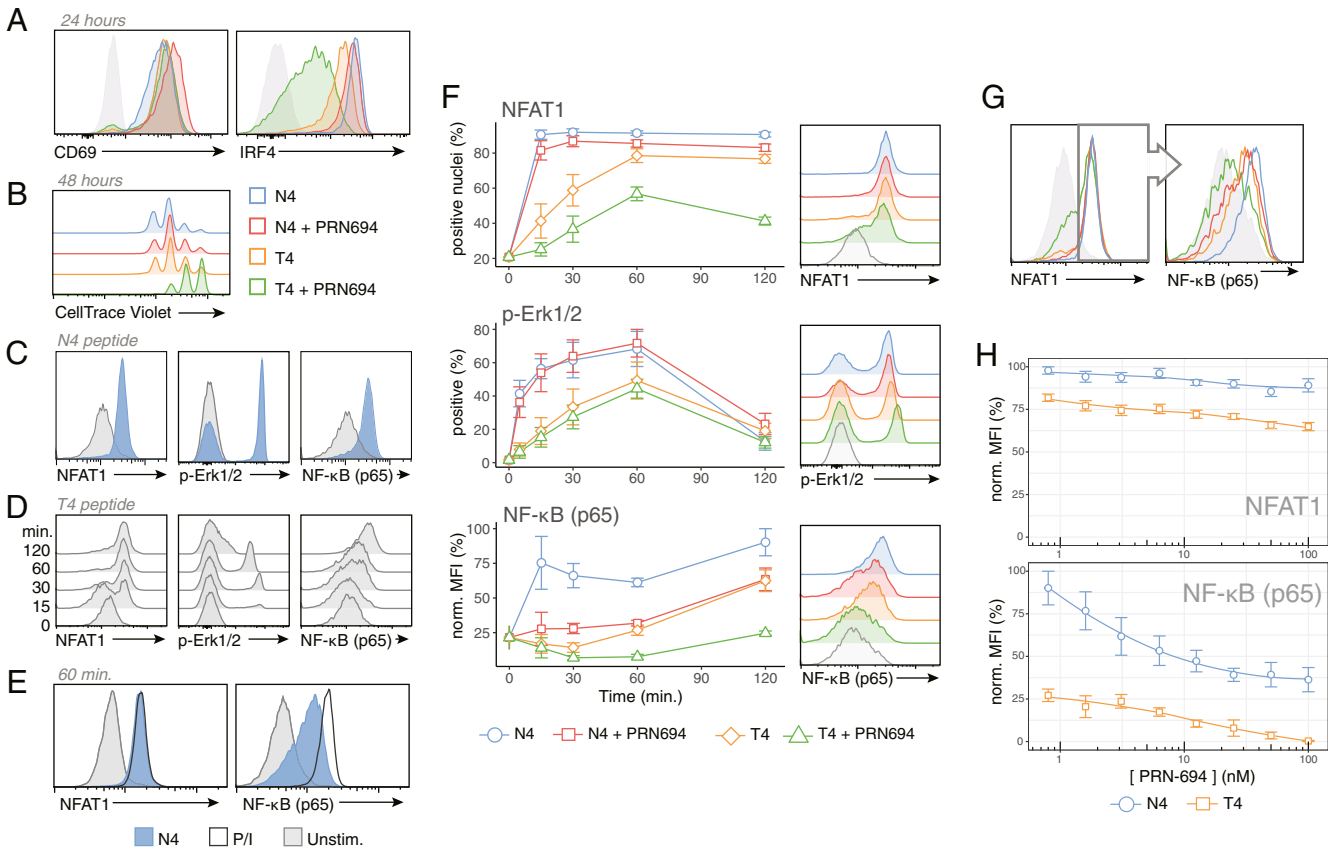

Fig. 1. TCR signal strength and PRN694 regulate-graded NF-κB activation within digitally NFAT1 and p-Erk active cells. (*A* and *B*) Histograms depicting CD69 and IRF4 expression after 24 h (*A*) or CellTrace Violet fluorescence after 48 h (*B*) in OT-I cells stimulated with APCs plus 100 nM indicated peptide with or without 50 nM ITK/RLK inhibitor PRN694. (*C*) Histograms of NFAT1 and NF-κB fluorescence in isolated OT-I nuclei or p-Erk1/2 fluorescence in OT-I cells after stimulation with APCs plus 100 nM N4 peptide stimulation for 1 h. (*D*) Histograms of NFAT1 and NF-κB fluorescence in isolated OT-I nuclei or p-Erk1/2 fluorescence in OT-I cells after stimulation with APCs plus 100 nM T4 peptide for the indicated times. (*E*) Histograms of NFAT1 and NF-κB (p65) fluorescence within OT-I nuclei isolated after 1-h stimulation with APCs plus 100 nM N4 OVA peptide or PMA (10 ng/mL)/Ionomycin (1 μM) addition. (*F*) Line plots depicting either NFAT1 or NF-κB fluorescence within OT-I nuclei or p-Erk fluorescence in OT-I cells over 2-h stimulation with APCs plus 100 nM indicated peptide with or without 50 nM PRN694. Histograms to the right represent nuclear or whole-cell fluorescence patterns after 60 min stimulation. (*G*) Histograms depicting NF-κB (p65) fluorescence within NFAT1+ nuclei after 1-h stimulation in conditions as in *A*, *B*, and *E*. (*H*) Line plots of change in normalized NFAT1 MFI (percentage) or normalized NF-κB (p65) MFI (percentage) within NFAT1+ OT-I nuclei after 1-h stimulation with APCs plus 100 nM N4 or T4 OVA peptide, in the presence of titrated concentrations of PRN694. Histograms shown are representative of three or more independent experiments.

ITK/RLK Inhibition Selectively Dampens NF-κB Intensity in Activating OT-I Cells. To test whether NF-κB activation was tunable by relative levels of ITK activity, we treated OT-I cells with the ITK/RLK inhibitor PRN694 prior to stimulation with peptide:MHC and then measured patterns of NFAT1 and NF-κB (p65) translocation or p-Erk1/2 induction. During N4 OVA peptide stimulation, ITK/RLK inhibitor treatment had little effect on NFAT1 and p-Erk1/2 activation but led to a marked reduction in the intensity of NF-κB activation (Fig. 1 *F* and *G*). Notably, NF-κB MFI was reduced in cells that had a similar amount of NFAT1 fluorescence as those from the untreated samples (Fig. 1*G*). NF-κB MFI was also more sensitive to incremental doses of PRN694 within NFAT1-positive nuclei (Fig. 1*H*). During stimulation with T4 peptide, inhibitor-treated cells had weakened NFAT1, p-Erk1/2, and NF-κB activation (Fig. 1 *F*–*H*). Various concentrations of strong N4, weak T4, or even weaker G4 peptide indicated that NF-κB activation was consistently sensitive to PRN964 treatment, while NFAT1 activation was less sensitive to PRN694, especially during strong N4 stimulation conditions (*SI Appendix*, Fig. S1 *A* and *B*). To confirm the specificity of PRN694 for ITK/RLK in T cells, we compared WT and $Itk^{-/-}$ OT-I cells stimulated in the presence or absence of PRN694 and measured NFAT1 and NF-κB (p65) nuclear translocation (*SI Appendix*, Fig. S1 *C* and *D*). As shown, these data confirm that PRN694 has no discernible effect on the response of $Itk^{-/-}$ OT-I cells, indicating its lack of off-target effects in T cells. Furthermore, these data also show that the PRN694 treatment of WT OT-I cells produces a similar inhibition of NFAT1 and NF-κB (p65) activation as observed with $Itk^{-/-}$ OT-I cells, indicating the complete, or near complete, inhibition of ITK signaling with this compound. Based on these data, we conclude that the overall effect of the inhibitor during weaker TCR signaling is to extend the temporal window during which cells "switched on," along with lowering the absolute probability, or threshold, of activation. Additionally, ITK/RLK inhibition mirrored the effect of varying TCR stimulation with weakened affinity peptides.

While NFAT activation is directly influenced solely by the activation of calcineurin, NF-κB can be regulated by both the DAG activation of IκB kinase (IKK) complex proteins as well as Ca^{2+} activation of CaM kinases (27, 30, 31). As ITK activity is upstream of both DAG and Ca^{2+}, ITK could possibly have multifactorial control over NF-κB activation. To separate DAG and Ca^{2+} components of NF-κB activation in OT-I cells, PMA or ionomycin was supplemented into wells of OT-I cultures during N4 stimulation with or without PRN694. The ionomycin addition to cultures during N4 stimulation did not modify the $NFAT1^{+}$ fraction (which was already >90% responders) or

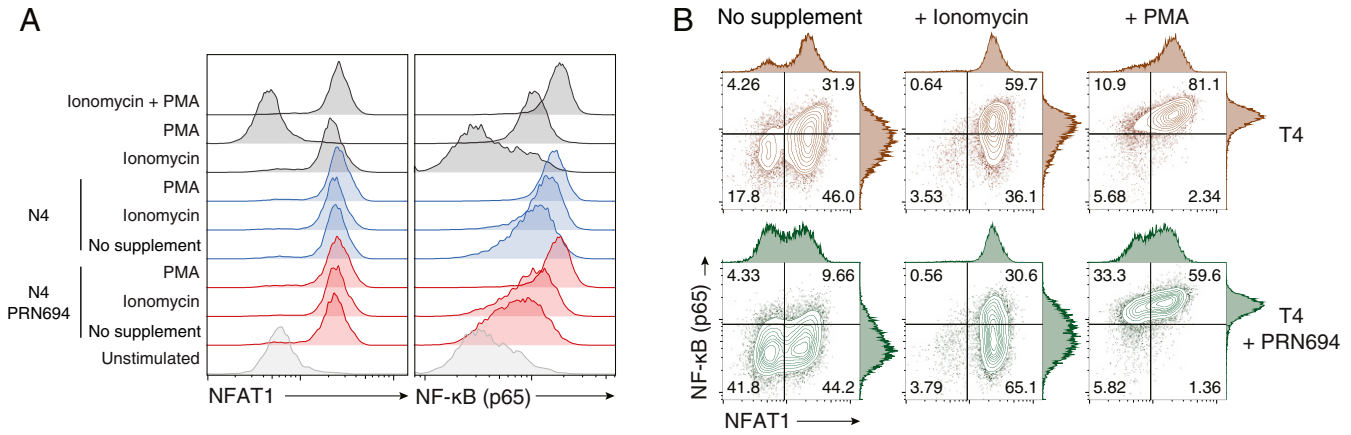

Fig. 2. PMA and ionomycin supplementation during peptide stimulation reveals synergistic NF-κB signaling activation. (*A*) Histograms depicting NFAT1 and NF-κB (p65) activation during 1 h 100 nM N4 stimulation with (red) or without (blue) 50 nM PRN694 or received no peptide stimulation (dark gray). A total of 1 μg/mL ionomycin or 12.5 ng/mL PMA supplemented to wells as indicated. (*B*) Fluorescence-activated cell sorting contour plots with adjust histograms comparing NF-κB (p65) and NFAT1 fluorescence after the same stimulation conditions as in *A* but with 100 nM T4 peptide stimulation.

modulate the NFAT1 fluorescence intensity (Fig. 2*A*) but did increase the proportion of NFAT1 responders during T4 stimulation, as expected (Fig. 2*B*). Ionomycin alone (in the absence of peptide stimulation) was sufficient to maximally translocate NFAT1 but did not induce appreciable NF-κB translocation (Fig. 2*A*). Ionomycin supplementation during N4 or T4 peptide stimulation increased NF-κB (p65) fluorescence intensity within individual nuclei, indicating that the threshold of Ca^{2+} flux sufficient to translocate NFAT1 is not the same as the maximum contribution to NF-κB translocation. PMA supplementation maximized NF-κB (p65) translocation in N4- or T4-stimulated cells and easily recovered the defect in NF-κB signaling because of ITK inhibition with PRN694. These experiments demonstrated that, under physiological peptide stimulation, separate downstream pathways are differently sensitive to the secondary messengers generated from the results of ITK activity. They also highlighted the synergistic nature of Ca^{2+} and DAG signaling in NF-κB activation but showed a dominant role for the amounts of DAG, rather than Ca^{2+}, to tune translocation.

These data demonstrated the complex behavior of concomitant signaling pathways in response to variable TCR inputs. We concluded that pathways such as NFAT1 and MAPK require a lower threshold of TCR stimulation to activate digitally, whereas NF-κB can be triggered rapidly (and appear digitally switched) under supraphysiological TCR engagement, but normal peptide stimulation produces a dynamic range of NF-κB activation states. Also, ITK activity is crucial in ensuring the optimal activation of graded NF-κB, which sheds light on the role of ITK as an amplifier of TCR signals.

ITK/RLK Inhibition Dampens NF-κB–Associated Gene Expression Immediately Following TCR Engagement. As we observed that NF-κB activation was more sensitive to ITK/RLK inhibition, we hypothesized that variable NF-κB intensities within activated cells might contribute to the immediate transcriptional control of graded gene induction. Prior to the up-regulation of effector genes like IL-2 and IRF4, activating $CD8^+$ T cells exiting a quiescent state undergo waves of primary and transient gene transcription (32–34). To connect observed differential signaling behavior in naïve T cells to immediate transcriptional effects, we treated OT-I cells with or without ITK/RLK inhibitor, briefly stimulated with OVA N4, and altered the OVA T4 peptide presented on WT splenocytes. We then sorted OT-I cells and measured the transcript abundance with RNA sequencing (RNA-seq).

To determine whether varying peptide affinity or modulating ITK activity regulated disparate transcriptional programming, we compared early up-regulated transcripts in N4- or T4-stimulated OT-I cells, with or without treatment, with ITK/RLK inhibitor at 30, 60, and 120 min of activation. We observed that each condition, testing different qualities of TCR signaling, induced sets of transcripts largely similar in composition but significantly different in abundance (Fig. 3 *A* and *B* and *SI Appendix*, Figs. S2 and S3). While a subset of transcripts that were identified in N4-stimulated cells were not significantly up-regulated in T4-stimulated cells, we found very few genes up-regulated in T4-stimulated cells that were not seen in N4-stimulated cells (*SI Appendix*, Fig. S3). We clustered genes induced over 2 h into six groups (Fig. 3 *A* and *B*). Gene clusters that exhibited peak expression 30 min after TCR contact with peptide:MHC were enriched for TCR signaling-related ontology terms, including "AP-1 signaling," "NF-κB signaling," and "NFAT signaling" (Fig. 3*C*). This suggested that TCR downstream signaling pathways directly regulate the transcription of these immediate early genes. Clusters of delayed genes first detectable at times greater than 30 min were enriched for terms linked to T cell effector functions "Myc targets" and cell cycle regulation, representing secondary gene transcription responses beyond immediate TCR control and likely regulated by a mix of continuing TCR signaling and first wave gene transcription. These experiments allowed us to interrogate the immediate transcriptional response to TCR engagement and revealed that the modulation of upstream TCR signal strength activates overall, similar transcriptional programming.

To determine whether weakened NF-κB activation during ITK/RLK inhibition differentially regulated the abundance of immediately induced transcripts, we compared differentially expressed transcripts in OT-I cells treated with or without inhibitor after 30 min of strong N4 peptide stimulation. Among transcripts significantly diminished by the ITK/RLK inhibitor were induced AP-1 family members (*Fos*, *Fosl1*, *Fosb*, and *Jun*) and NF-κB response genes (*Nfkbia*, *Nfkbid*, *Nfkbiz*, and *Tnfaip3*) (Fig. 4*A*). We interpret these results as reflecting the effect of weakened NF-κB signaling in ITK-inhibited cells. Genes that were up-regulated, compared with unstimulated cells, but were less sensitive to ITK/RLK inhibition included Egr family transcripts (*Egr1*, *Egr2*, and *Egr3*) and the activation marker CD69 (Fig. 4*A*). After 2 h stimulation, ITK/RLK inhibitor-treated OT-I T cells also had a significantly lower expression of cytokines (*IL2* and *Ifng*) and effector-associated transcripts (*Irf4*), consistent with the known importance of ITK signaling in promoting robust

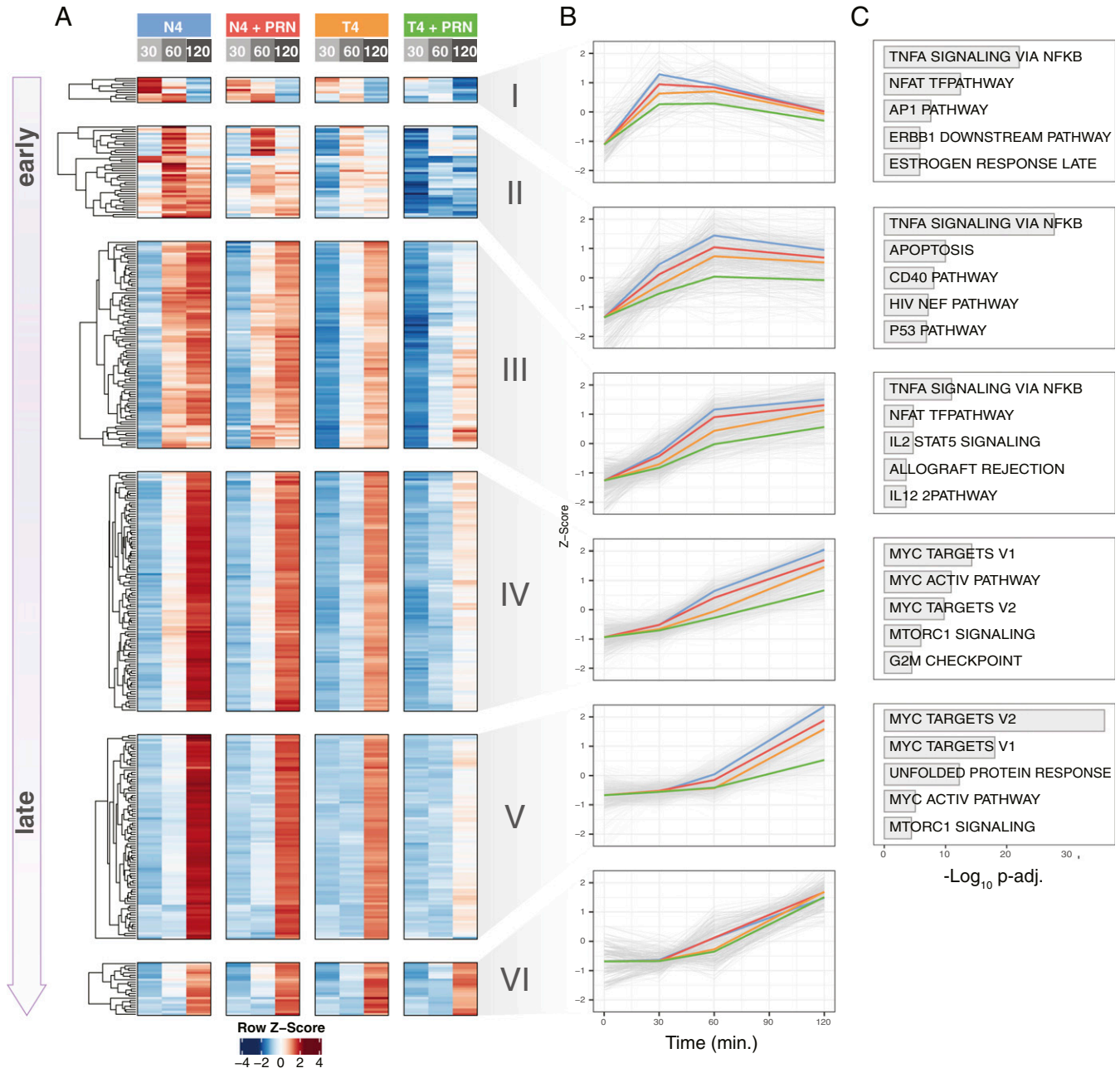

Fig. 3. Inhibition of ITK dampens immediate TCR signaling-induced transcripts. (*A*) Heatmap depicting mean variance-stabilized transformed normalized expression values of top 357 genes (Log2 fold change > 2, mean expression > 1,000, and *P* adjusted [*p*-adj.] < 0.1) induced in OT-I CD8+ T cells at three timepoints (30, 60, and 120 min) after stimulation with APCs plus 100 nM N4 OVA or T4-altered OVA peptide with or without 50 nM PRN694. Genes were grouped with *k*-means clustering into six clusters. (*B*) Line plots depicting *z*-score of 2-h expression time course of gene clusters identified in *A*. Scores for mean expression values for each cluster are grouped by conditions in *A*: N4 (blue), N4 + PRN694 (red), T4 (orange), and T4 + PRN964 (green). Total expression data for all conditions from three replicates are drawn in gray. (*C*) Enriched Molecular Signatures Database (MSigDB) signatures in gene clusters identified in *A*. Log10 transformed adjusted *P* values (false discovery rate) of (up to) the top five terms (*p*-adj. ≤ 0.05) from both "Hallmark Gene Sets" and "Immunologic Signatures" MSigDB collections. Cluster VI did not contain gene set enrichments with these constraints. Data represent three separate biological replicate experiments each utilizing pooled splenocytes from three or more OT-I mice.

effector T cell functions (*SI Appendix*, Fig.S4) (35–37). Independent of TCR stimulus, most immediately induced transcripts (e.g., *Fos*, *Fosb*, *Fosl1*, *Egr1*, and *Egr2*) peaked in abundance 30 min after contact with peptide:MHC (Figs. 3 *A* and *B* and 4*A* and *SI Appendix*, Fig. S4). This window of transcription is a known pattern of immediate early gene regulation (33, 34). Our RNA-seq experiments did not suggest that the ITK/RLK inhibitor caused a delayed induction of these genes in strongly stimulated OT-I cells, but effects of this type might be revealed by further single-cell expression analysis approaches.

Changes in DNA Accessibility Sensitive to ITK/RLK Inhibitor Are Enriched for NF-κB and AP-1 Motifs. To connect individual TCR signaling pathway behavior with the ITK control of immediate gene expression patterns, we measured immediate, genome-wide DNA accessibility changes with an assay for transposase-accessible

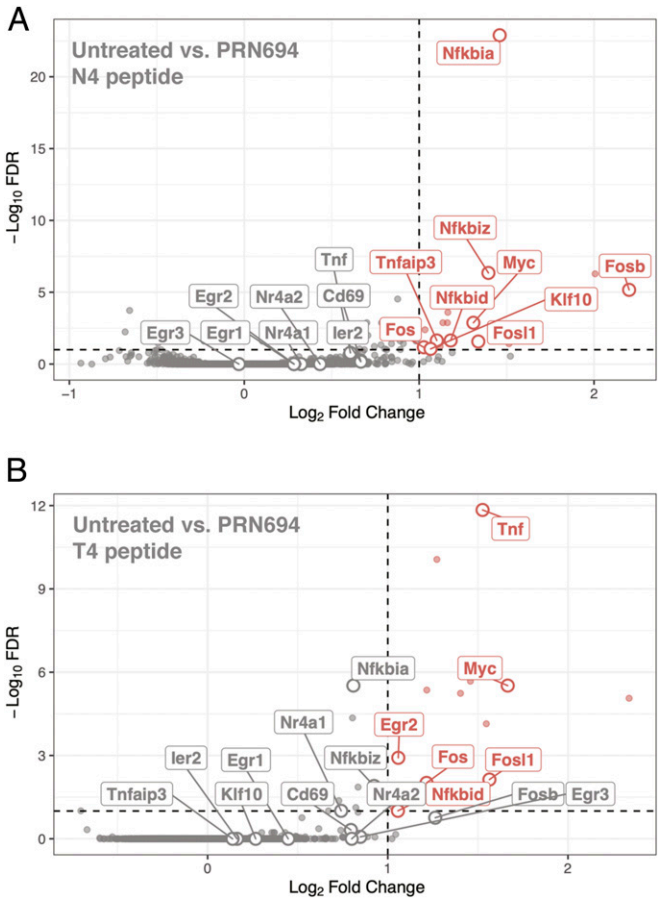

Fig. 4. Immediate transcripts are differentially sensitive to PRN694 treatment. (*A* and *B*) Volcano plots identifying transcripts sensitive to 50-nM PRN694 treatment measured after 30 stimulation of OT-I cells with APCs plus 100 nM N4 peptide (*A*) or 100 nM T4 peptide (*B*). Labeled gene names represent select early induced transcripts significantly expressed, compared with unstimulated controls, extracted from either clusters I or II from Fig. 3. Plots depict the Log_2 fold change of normalized expression of untreated samples over PRN694-treated samples against −Log10 transformed false discovery rate (FDR) values. Data points and gene names significantly above fold change cutoffs (Log2 fold change > 1 and −Log10 FDR < 0.1) are drawn in red; genes that were not significantly differentially expressed because of PRN694 treatment are drawn in gray.

chromatin and sequencing (ATAC-seq). (38). Cells for ATAC-seq analysis were sorted at the same time as those used in RNA-seq experiments to better compare accessibility changes with gene expression. Principal component analysis of ATAC-seq replicates indicated that variance was attributed to differences in stimulation (*SI Appendix*, Fig. S5). Compared with naïve, unstimulated OT-I cells, strong N4 stimulation induced the most significant differences in DNA accessibility, most evident after 120 min (Fig. 5*A*). After only 30 min of N4 stimulation, about 10,000 DNA regions displayed differential accessibility compared with unstimulated cells (Fig. 5*B*). To evaluate differential accessibility due to ITK inhibition, N4-stimulated cells with and without ITK inhibition were compared. After 30 min stimulation, the most significant changes in accessibility due to PRN694 were found near many gene loci also identified in early transcriptional data, including AP-1 factors (*Fosb* and *Jun*), NF-κB response genes (*Nfkbia* and *Nfkb1*), and genes encoding transcription factors important in regulating effector function (*Rel*, *Nfatc1*, and *Irf4*) (Fig. 5*C*). This indicated that while many genomic regions change in accessibility similarly during activation, the few that were most sensitive to PRN694 were near early genes that echoed the most sensitive gene sets found in the transcriptional analysis.

Like the RNA-seq experiments, the strength of the TCR stimulation or ITK/RLK inhibition did not regulate an independent set of genomic regions but rather regulated the intensity of a shared set of activation-associated pileups (Fig. 5 *E* and *F*). *k*-means clustering of all dynamic ATAC-seq peaks (differentially accessible compared with unstimulated control) after 30 min stimulation revealed the regulation of regions that had increased dependency on ITK activity (Fig. 5*D*). We performed Hypergeometric Optimization of Motif EnRichment (HOMER) analysis to identify motif enrichments unique within each cluster, compared with a background of reciprocal clusters (39). Cluster 1, which appeared to represent regions that were less accessible during treatment with the ITK/RLK inhibitor, was significantly enriched for AP-1 (Fosl2) motifs and NF-κB (p65) motifs. Gene ontology analysis using gene annotations nearest to each ATAC peak revealed that Cluster 1 was enriched for genes associated with NF-κB and Stat5 signaling (*SI Appendix*, Table S1). Cluster 2, which contained genomic regions less sensitive to PRN694 treatment, were significantly enriched for NFAT motifs (Fig. 5*D*).

We performed Fisher's exact test to calculate the amount of overlap of genomic regions in each ATAC-seq cluster with publicly available transcription factor chromatin immunoprecipitation sequencing (ChIP-seq) datasets (Fig. 5*D*). This revealed that Cluster 2 had a strong association (3.23) with WT NFAT1 ChIP-seq, while Cluster 1 (0.83) and Cluster 3 (0.01) did not. Cluster 2 also had a strong overlap (2.57) with ChIP-seq peaks generated from NFAT1 knockout mice transferred with constitutively active, mutant NFAT1 that cannot bind with AP-1 (CA-RIT-NFAT1) (40). NF-κB (p65) ChIP-seq peaks had a similar, strong association (>3.0) with Clusters 1 and 2. Overall, ATAC-seq analysis revealed that specific DNA genomic regions least sensitive to varied signal strength via peptide avidity or PRN-694 treatment were associated with NFAT regulation, while regions most sensitive to PRN-694 were associated with AP-1 and NF-κB regulation.

TCR Stimulus and ITK Regulate-Graded Selective Expression of Early Gene Products. To determine whether ITK/RLK inhibitor-specific effects on immediate transcription also led to reduced protein product accumulation during activation, we measured Egr2, c-Fos, and c-Myc intracellular content in stimulated cells via flow cytometry (Fig. 6 *A*–*C*). Both c-Fos and Egr2 proteins were detectable within 30 min after OVA stimulation. Treatment with the ITK/RLK inhibitor dampened the amount of c-Fos expression in OVA-stimulated OT-I cells but had little effect on modulating Egr2 expression. After approaching a peak expression at 60 min, the expression of both proteins was stable out to 6 h. This indicated that ITK/RLK-inhibited OT-I cells did not "catch up" in c-Fos expression during the time course of this experiment, and the RNA-seq experiments measured dampened expression and not an average of asynchronous cells. Cells that expressed both CD69 and Egr2 also displayed a graded amount of c-Fos expression dependent on the TCR stimulation strength and ITK/RLK inhibition (Fig. 6*D*). These results also confirmed that ITK/RLK signaling contributes to graded gene expression in response to variations in TCR signal strength.

NF-κB Inhibition Produces Graded Immediate Gene Expression. To test whether a selected gene exhibiting graded induction during the first 30 min after stimulation was NF-κB dependent, we treated OT-I cells with either an inhibitor of the IKK complex, IKK-16, or for comparison, an MEK inhibitor (PD325901) to control activation of MAPK (Erk1/2). As expected, neither IKK-16 nor PD325901 had an effect on NFAT1 translocation in OT-I cells (*SI Appendix*, Fig. S6 *A* and *B*), but treatment with the IKK-16–tuned NF-κB (p65) translocation and treatment of PD325901 effectively inhibited p-Erk (*SI Appendix*, Fig. S6 *A* and *B*).

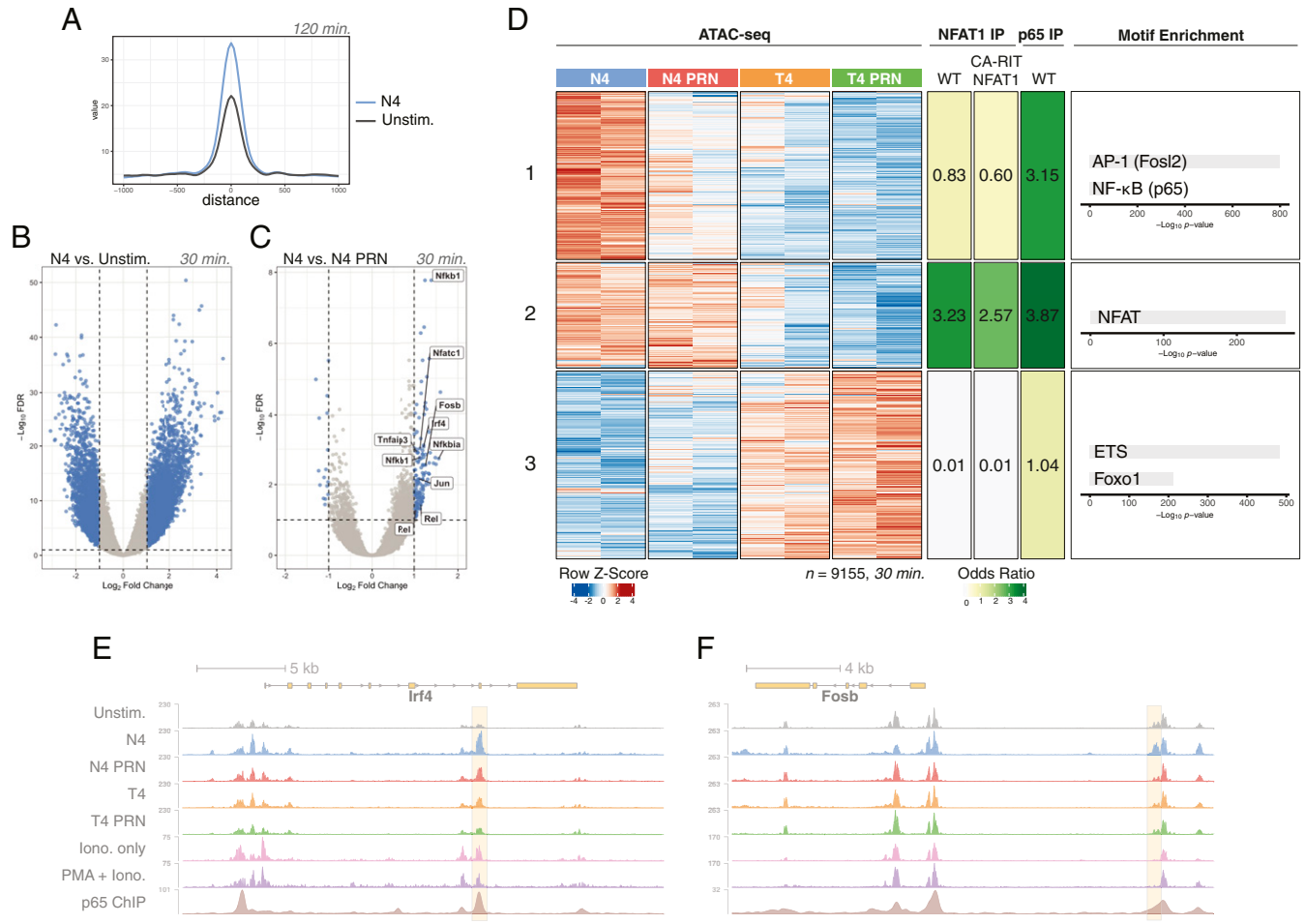

Fig. 5. Early ITK-dependent changes in DNA accessibility are associated with NF-κB and AP-1 regulation. (*A*) Distribution of ATAC-seq fragment distance from peak centers. Comparison of 120-min stimulation with N4 peptide (blue) and unstimulated OT-I nuclei (gray). (*B*) Volcano plot of differentially accessible genomic peak regions after 30 min stimulation with N4 peptide. (*C*) Volcano plot of differentially accessible peak regions due to PRN694 treatment after 30 min of N4 peptide stimulation. Annotations of the closest gene TSS are labeled for select regions. For *B* and *C*, significantly differentially accessible regions (Log_2 fold change < −1 or > 1 and *P* adjusted [*p*-adj.] < 0.1) are drawn blue. (*D*) Heatmap depicting *k*-means clustering ($k = 3$) of row-scaled coverage for dynamic peaks (|Log2 fold change| > 1 and *p*-adj. < 0.01) after 30 min. A total of 100 nM N4 or T4 peptide stimulation with or without 50 nM PRN694 (N4 untreated, blue; N4 + PRN694, red; T4 untreated, orange; and T4 + PRN694, green). To the right are the calculated Fisher's Exact Test odds ratios indicating the amount of overlap of peak regions within each ATAC cluster with public ChIP-seq datasets, including NFAT1 immunoprecipitation (IP) from either WT NFAT1 mouse $CD8^+$ T cells (WT) or NFAT1 KO $CD8^+$ T cells transduced with constitutively active mutant NFAT1 unable to interact with AP-1 (CA-RIT-NFAT1) after 1-h PMA and ionomycin stimulation (40, GSE64409) and p65 IP after 3-h anti-CD3/CD28 simulation of mouse T cells (67, GSE82078). Also adjacent to each cluster is HOMER de novo motif enrichment analysis, presenting top (*p*-adj. < 10^{-50}) motifs for each cluster. (*E* and *F*) ATAC-seq genomic tracks for regions around *Irf4* and *Fosb* loci, comparing different peptide and PRN694 stimulation conditions after 30 min. Also plotted are ionomycin or ionomycin + PMA stimulation ATAC-seq peaks and NF-κB ChIP-seq peaks (67, GSE82078 and 69, GSE93014). Select, differential, and experimental ATAC-seq peaks are highlighted in yellow.

Examination of c-Fos expression revealed that OT-I cells treated with moderate concentrations of IKK-16 or PD325901 showed dampened c-Fos expression (*SI Appendix*, Fig. S6 *A*, *C*, and *D*). In contrast, expression of Egr2, a gene with an all-or-nothing expression profile, was inhibited by PD325901 treatment but was largely unaffected by IKK-16 treatment. For instance, at 1 h poststimulation, Egr2 expression was unchanged in the presence of IKK-16, whereas c-Fos expression was reduced twofold (*SI Appendix*, Fig. S6 *C* and *E*). These experiments indicate that the induction of select, immediate genes, such as c-Fos, reflect graded amounts of NF-κB during activation.

Discussion

Our results provide evidence for a hierarchy of signaling thresholds for pathways downstream of the TCR and ITK. NFAT, MAPK, and NF-κB signaling all exhibit varying patterns of activation in single, naïve OT-I cells after stimulation with OVA peptide or altered OVA peptide ligands. We found that NF-κB p65 translocation is uniquely sensitive to the quality of peptide:MHC interaction and ITK/RLK activity (Fig. 7). Our findings also demonstrated that diminished NF-κB signaling due to ITK/RLK inhibition has transcriptional effects in stimulated T cells, in that NF-κB response genes and induced AP-1 gene family (*Fos*, *Fosl1*, and *Fosb*) members are diminished in abundance compared with untreated cells. While previous studies have shown a key role for BTK in activating NF-κB downstream of the BCR and BAFF receptor in B cells (41–43), our studies reveal the additional, important element that graded NF-κB activation is regulated by the magnitude of ITK kinase activity in T cells.

Most models of TCR initiation describe receptor proximal signaling as digital and inherently noisy. In order for successful TCR signaling to result in changes to transcription factor activation in the nucleus, pathways must produce stable intermediates only after repeated and sustained engagements with peptide:MHC

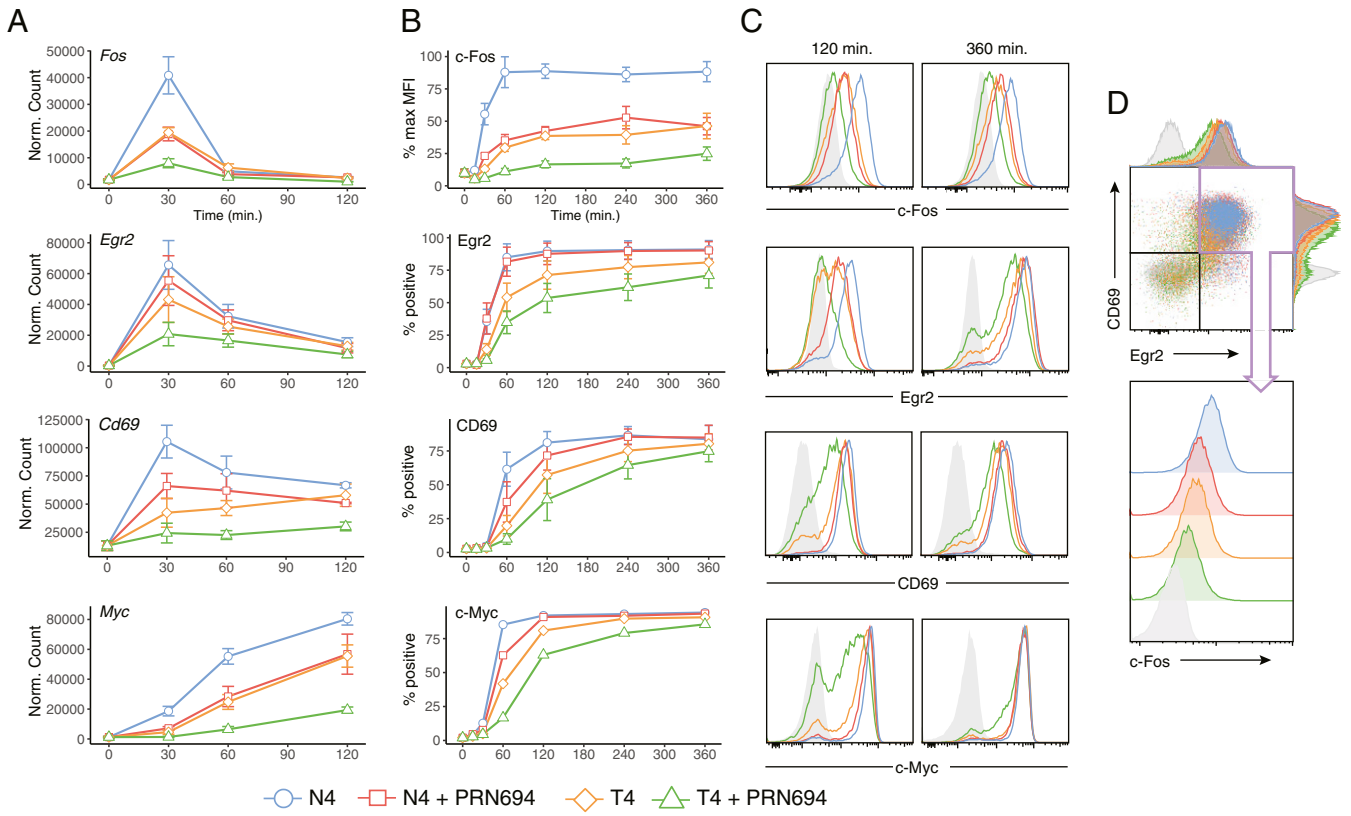

Fig. 6. TCR signaling and ITK control-graded accumulation of early gene product c-Fos. (*A*) Line plots of mean-normalized expression counts of select induced transcripts measured at 0, 30, 60, and 120 min. (*B* and *C*) Line plots (*B*) and representative histograms (*C*) of flow cytometry results for gene products of transcripts profiled in *A*. Experiments were conducted under similar stimulation conditions and previous figures and stimulated up to 6 h. Results are plotted as percentage positive or normalized to maximum MFI (percent max MFI) where indicated. (*D*) Representative histograms depicting graded c-Fos fluorescence in CD69$^+$ Egr2$^+$ OT-I cells in response to different stimulation conditions measured after 6 h. Labeling is consistent: N4—blue (circles), N4 + PRN—red (squares), T4—orange (diamonds), and T4 + PRN694—green (triangles). Data represent three biological replicates. Error bars indicate SEM.

(5, 11, 44). TCR-induced MAPK activation has been shown to exhibit strong digital behavior due to the positive feedback regulation of son of sevenless (SOS), which sustains active Ras (12, 44). To measure activation of MAPK signaling, we observed p-Erk1/2 fluorescence in single cells with flow cytometry. Consistent with previous reports, we measured strongly digital Erk activation in response to TCR ligation with peptide:MHC (11, 12). The fraction of cells positive for p-Erk after PRN694 treatment remained largely unchanged, but the p-Erk fraction was sensitive to peptide affinity (Fig. 1*F*). We expected p-Erk fluorescence to be sensitive to ITK activity because DAG production stabilizes SOS activation (12). However, it is possible that upstream phosphorylation of LAT after TCR triggering is the rate-limiting step for MAPK activation rather than the ITK-dependent production of DAG. Furthermore, initial experiments with *Itk*$^{-/-}$ mice reported decreased p-Erk in pooled whole CD8$^+$ T cell lysates after stimulation with anti-CD3 antibody (21). In contrast, our experiments measure TCR responses after engagement with peptide:MHC ligands, which show markedly different kinetics compared with those elicited by α-CD3 stimulation.

A separate study previously reported NF-κB behaves digitally after TCR stimulation. Direct antibody-mediated stimulation of the TCR in C57BL/6 mouse CD4$^+$ and CD8$^+$ T cells or OVA peptide stimulation of CD4$^+$ OT-II cells displayed evidence of digital NF-κB activation (13). In the current study, we provide a carefully tuned examination of physiological NF-κB responses in naïve CD8$^+$ T cells. Given sufficiently strong peptide stimulation (native N4 OVA peptide) or PMA/Ionomycin, T cells can quickly and completely translocate p65 with similar kinetics as NFAT1, appearing "all or none" (Figs. 1 *C* and *E* and 2*A*). Our results reveal, however, the strength of TCR stimulation the amount of ITK activity produces intermediate, graded states of p65 activation during T cell priming.

As we observed that NF-κB signaling was specifically sensitive to PRN694 treatment, these findings highlighted a role for ITK in amplifying signals induced by weaker TCR inputs that could not sufficiently trigger NF-κB on their own, even under conditions that stimulate NFAT and Erk. Later during activation, after initial priming, combined TCR, CD28, and other costimulatory receptors become increasingly important in amplifying NF-κB signaling via PI3K (45). It may be advantageous for naïve cells to limit NF-κB by making it more difficult to trigger with TCR stimulus alone. Our results reveal, however, that weaker TCR stimulation or ITK/RLK inhibition with PRN694 produces intermediate states of p65 activation, which do not appear digital. Robust p65 nuclear translocation requires ITK and strong TCR interaction; in contrast, NFAT1 and p-Erk remain digitally responsive during weaker TCR stimulation or PRN694 treatment, with the amounts of nuclear NFAT1 and p-Erk equivalent to those observed after strong TCR signaling. These results indicate discrete, analog levels of NF-κB activation during T cell priming.

NFAT translocation is exclusively dependent on SOCE activation of calcineurin, while NF-κB activation is layered with multiple signaling inputs (28, 46, 47). ITK and the subsequent PLC-γ1–induced production of DAG activates NF-κB p65 through PKC-theta (17, 28). PLC-γ1 production of IP_3 generates

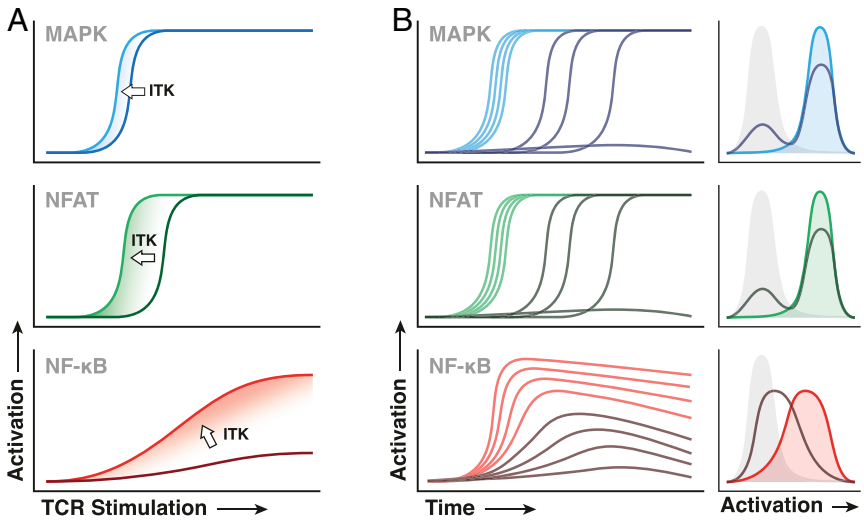

Fig. 7. Data summary of TCR signal strength effects on the activation of separate signal pathways. (*A*) Line plots depicting how ITK disproportionately shifts signaling thresholds. MAPK, NFAT, and NF-κB responses are drawn in blue, green, and, red, respectively. Activation response when ITK is present is drawn in a lighter shade; activation without ITK is drawn in a darker shade. Direction of the shift due to the presence of ITK is indicated with an arrow. TCR stimulation input is plotted against the resultant degree of activation. (*B*) Summary of TCR signal strength control of pathway activation within a stimulated population. Groups of curves representing single-cell MAPK (blue), NFAT (green), and NF-κB (red) responses to either strong (light shade) or weak (dark shade) stimulation are presented over time. Histograms to the right represent the cumulative distribution of pathway activation of the populations in the line plots.

a calcium flux and activates calmodulin and subsequently calcineurin, which dephosphorylates sequestered NFAT1. Calmodulin also activates calmodulin-dependent protein kinases, which can stabilize the CARMA complex and ultimately assist in NF-κB activation (48). Thus, ITK influences the activity of NF-κB by both DAG and IP_3 production. Experiments with ionomycin alone stimulate modest NF-κB p65 activation in naïve T cells, albeit lessened compared with TCR stimulation with peptide:MHC (Figs. 1*E* and 2). We and others describe digital NFAT1 translocation and calcium flux in single cells, in which a discrete threshold of activation governs an all-or-none response (Fig. 1 *C* and *D*) (7, 9, 10). We attribute the sensitivity and analog qualities of NF-κB activation, in response to ITK activity, to the combinatorial effects of simultaneous Ca^{2+} and DAG signaling (Fig. 2). Indeed, higher NF-κB MFI correlates with "switched on" NFAT1 fluorescence, indicating that digital TCR initiation and Ca^{2+} flux may precede NF-κB activation (Fig. 1 *C*, *E*, and *F*).

One of the questions driving our transcriptomics and genomics experiments was to discern whether ITK activity and, broadly, the strength of TCR signal directs diverging transcriptional programs or rather tunes the abundance of transcripts within one activation-associated gene set. RNA-seq results revealed that ITK inhibition or weaker TCR interactions with lower-affinity peptide:MHC induce similar genes as strong TCR signaling (Fig. 3). A recent single-cell, transcriptomic study thoroughly concluded that peptide-stimulated OT-I cells activate a single-effector transcriptional program, and resultant effector cells have similar cytolytic capacity, independent of TCR signal strength (24). With single-cell RNA-seq analysis, the same study also showed that weaker TCR signaling delays early gene transcription. We identified the temporally induced early gene clusters within 2 h TCR stimulation but did not detect similar shifts in transcriptional kinetics due to ITK inhibition or weaker peptide affinity, but this is likely a limitation of our pooled RNA-seq experiments. In contrast, our analyses of signaling events in naïve OT-I cells do show weaker stimulation and ITK inhibition delays onset of peak fractional NFAT responders, and NF-κB is only appreciably detectable after 60 mins. Additionally, cytometric analysis of CD69, c-Myc, Egr2, and c-Fos display reduced kinetics of expression when stimulated with weak peptide:MHC.

Cooperation of NFAT, AP-1, and NF-κB transcription factors is required for many aspects of optimal transcription of T cell activation programming, including production of cytokines like IL-2, which was one of the most differentially expressed genes because of TCR signal strength or PRN694 treatment after 2 h (*SI Appendix*, Fig. S4). Early IL-2 signaling through the induced, high-affinity IL-2 receptor CD25 helps maintain levels of c-Myc, while also lowering the apparent TCR signaling threshold (49, 50). Thus, $CD8^+$ T cells that quickly transcribe large amounts of IL-2 can maximize their clonal expansion. The IL-2 promoter contains NF-κB binding sites and critical NFAT:AP-1 binding sites, in which both partners are required for transcription (33). In ITK-inhibited cells or during weak signaling, we measure reduced NF-κB activation, diminished production of AP-1 transcripts (*Fos*, *Fosb*, and *Fosl1*), and decreased Fos protein (Fig. 4). These conditions could contribute to the slower production of IL-2 transcripts, which are among the most sensitive to the strength of TCR within 2 h. There is evidence that T cells may continue to accumulate c-Fos proteins after serial encounters with APCs during the early periods of T cell priming, effectively summing their cumulative duration of signaling (51, 52). TCR stimulation that induces efficient NFAT translocation, but not NF-κB, and only weakly induces AP-1 factors may suffer from the low accumulation of early gene products and weak IL-2 production. ChIP assays utilizing a constitutively active NFAT mutant, in which NFAT is permanently nuclear, shows that NFAT cannot bind the IL-2 promoter without its AP-1 binding partner; in the absence of AP-1, IL-2 transcription is abrogated (40, 53).

A better understanding of the biology of T cell exhaustion is crucial in treating chronic illness and maximizing the efficacy of T cell immunotherapies, such as CAR-T. Recent work has identified NFAT as an important TCR-dependent regulator of T cell exhaustion phenotypes (40, 53, 54). NFAT can bind to the promoter of select exhaustion-associated genes without its partner AP-1 (40) and drives the expression of NR4A family transcription factors, which further maintain exhaustion programming (53, 54). Within the hierarchy of T cell signaling pathways we identify here, NFAT and MAPK appear to be more easily stimulated than NF-κB. Our data provide further evidence that CD8 T cells may signal

through NFAT more easily without complete downstream pathway activation, which could contribute to exhaustion phenotypes.

Materials and Methods

Mice. Mice were bred and housed in a specific, pathogen-free facility at the University of Massachusetts Medical School and the University of Colorado-Anschutz School of Medicine, in accordance with Institutional Animal Care and Use Committee guidelines. OT-I transgenic *Rag1*$^{-/-}$ mice (B6.129S7-Rag1^{tm1Mom} Tg(TcraTcrb)1100Mjb N9+N1) and C57BL/6 WT mice were purchased from Taconic Biosciences. OT-I *Itk*$^{-/-}$ *Rag1*$^{-/-}$ mice were generated by crossing OT-I *Rag1*$^{-/-}$ and *Itk*$^{-/-}$. *Itk*$^{-/-}$ mice have been described previously (19). CD45.1^{+} (B6.SJL-PtprcaPep3b/BoyJ) mice were purchased from the Jackson Laboratory. Unless otherwise noted, experimental cohorts consisted of age- and sex-matched littermates aged 6 to 12 wk.

Stimulation of CD8^{+} T Cells. Freshly harvested OT-I *Rag1*$^{-/-}$ mouse splenocytes were pooled, red blood cell (RBC) lysed, and enriched for CD8^{+} cells with an EasySep negatively selective magnetic isolation kit (STEMCELL Technologies). OT-I cells prepared for use in nuclei isolation experiments were then treated with CellTrace Violet reactive dye (Invitrogen) for 20 min to fluorescently label cells (including nuclei). OT-I cells were cultured at 2×10^5 cells per well (unless otherwise noted) and incubated with or without 50 nM (or otherwise noted) ITK/RLK inhibitor PRN694 (Principia Biopharma) for 30 min at 37 °C. In some experiments, OT-I cells were incubated with or without IKK inhibitor IKK-16 (Sigma) or MEK inhibitor PD325901 (Tocris Bioscience). For APCs, RBC-lysed splenocytes harvested from WT mice were cultured at 4×10^5 per well and incubated with indicated concentrations of OVA "N4" peptide (SIINFEKL), altered OVA "T4" peptide (SIITFEKL), and altered OVA "G4" peptide (SIIGFEKL) (21st Century Biochemicals) for 30 to 60 min at 37 °C. OT-I cells and peptide-loaded splenocytes were then combined and incubated at 37 °C for specific times. For cell preparations used for molecular analyses (e.g., RNA-seq and ATAC-seq analyses), splenocytes from CD45.1^{+} WT mice were used as peptide-presenting cells for easy exclusion from CD45.2^{+} OT-I cells via cell sorting.

Nuclei Isolation. To measure the translocation of nuclear proteins, we isolated cell nuclei after stimulation for fixation and subsequent flow cytometry analysis. To do this, we utilized a sucrose buffer-based protocol that we and others have previously published (7, 10). To summarize, stimulated cells were pelleted and washed with 200 μL of ice-cold "Buffer A" containing 320 mM sucrose, 10 mM Hepes (Life Technologies), 8 mM $MgCl_2$, 13 EDTA-free cOmplete Protease Inhibitor (Roche), and 0.1% (volume/volume) Triton X-100 (Sigma-Aldrich). After 15 min on ice, the plate was spun at 2,000× *g* and 4 °C for 10 min. This was followed by 2× 200 μL washes with "Buffer B" (Buffer A without Triton X-100) at 2,000× *g* and 4 °C.

Antibodies and Flow Cytometry. Stimulated cells and isolated cell nuclei were fixed and permeabilized with the Foxp3/Transcription Factor Staining Buffer Set (eBioscience), except cells used for anti-p-Erk1/2 analysis, which were fixed with 4% paraformaldehyde (Electron Microscopy Services) and permeabilized with 90% ice-cold methanol (Fisher Scientific). Fluorescently labeled flow cytometry antibodies against IRF4 (3E4), CD69 (H1.2F3), and Egr2 (erongr2) were purchased from eBioscience. Antibodies against CD8a (53-6.7), CD8b (53-5.8), CD25 (3C7), CD90.2 (53-2.1), and p-Erk1/2 (4B11B69) were purchased from BioLegend. Antibodies against NFAT1 (D43B1), NF-κB p65 (D14E12), c-Fos (9F6), and c-Myc (D84C12) were purchased from Cell Signaling Technology. Anti-CD45.1 (A20) was purchased from BD Pharmingen. PE-conjugated F(ab')2-goat anti-rabbit IgG (H+L) cross-adsorbed secondary antibody was purchased from Invitrogen.

Cell Sorting. Samples of stimulated CD45.2^{+} OT-I cells and CD45.1^{+} WT splenocytes mixtures were stained with CD8a and CD45.2 antibodies, and 7-AAD and OT-I cells were sorted using fluorescence-activated cell sorting (FACS) (BD FACSAria) into 100% fetal bovine serum (FBS) and pelleted.

RNA-Seq Library Preparation. Total RNA from ~300,000 OT-I cells per sample was collected with the RNeasy micro kit (Qiagen) with a 15-min on-column DNase digestion (Qiagen) to remove genomic DNA. Total RNA quality and quantity was determined with fragment analysis (University of Massachusetts Medical School Molecular Biology Core Laboratory) and Qubit Fluorometer (Invitrogen) analysis. Complementary DNA libraries were generated following a modified, paired-end switching mechanism at 5′ end of RNA template (SMART) sequencing protocol (55, 56). Briefly, at least 20 ng input RNA was used for reverse transcription with SMARTscribe reverse transcriptase (Clontech). Whole transcriptome amplification (WTA) was performed with Advantage 2 polymerase (Takara Bio). WTA reactions were monitored with qPCR to determine optimal cycle number. WTA libraries were then size selected with AMPure XP DNA solid phase reversible immobilization (SPRI) beads (Beckman Coulter), tagmented with Tn5 transposases (Illumina Nextera XT), barcoded, and amplified with a cycle number determined via qPCR monitoring. Final libraries were further size selected with SPRI beads to an average size of 300 to 500 bp, and quality was assessed with fragment analysis and Qubit analysis. Libraries were pooled and sequenced on a NextSEq. 500 sequencer (Illumina).

Processing and Analysis of RNA-Seq Reads. Adapter sequences were trimmed from quality raw sequencing reads with Trimmomatic-0.38 (57) and then aligned to mouse ribosomal RNA with Bowtie2 version 2.3.2 (58). Unaligned reads were retained, and gene expression was estimated (transcripts per million and expected counts) with RSEM version 1.2.29 (59) configured to align to an mm10 RefSeq transcriptome with Bowtie2 version 2.3.2. Samples were filtered to retain expressed genes (expected counts >200), and batch effects between replicates were corrected with limma version 3.42.2 (60). Differential expression analysis was performed with DESeq2 version 1.26.0 (61) to identify induced genes (stimulated conditions versus unstimulated controls) or condition-specific changes in expression (untreated versus PRN694 or N4 versus T4 OVA peptides). Hierarchical clustering and *k*-means clustering of differentially expressed genes was performed within R version 3.5. Heatmap visualizations of gene clusters were drawn with ComplexHeatmap (62).

Gene Ontology. We utilized the R packages msigdbr version 7.0.1 and clusterProfiler version 3.18.1 (63) to compare clusters of differentially expressed genes with the Molecular Signatures Database Hallmark (H) and Immunologic (C7) gene sets (60–62). The top five terms with false discovery rate <0.05 were displayed in *Results*.

ATAC-Seq Library Preparation. Precisely 50,000 stimulated OT-I T cells were FACS sorted (BD FACSAria) at the same time as RNA-seq samples and pelleted in 100% FBS. ATAC-seq libraries were generated similarly, as described in Buenrostro et al. (38). Briefly, cell nuclei were isolated and transposed with 8 μL Tn5 (Illumina Nextera) at 37 °C for 60 min. DNA fragments were isolated with a Clean and Concentrator Kit (Zymo) and then Illumina barcoded and amplified with NEBNext High-Fidelity 2× PCR Master Mix (New England Biolabs). A portion of the reaction was performed as a separate qPCR reaction to determine the ideal cycle number. Samples were then size selected with SPRI beads to include fragments up to 450 bp, ensuring to maintain small (<200 bp), nucleosome-free fragments. The quality of final ATAC-seq libraries was assessed with fragment analysis and Qubit analysis. Libraries were then pooled and sequenced on an Illumina NextSEq. 500.

Alignment and Processing of ATAC-Seq Reads. Adapter sequences were trimmed from raw sequencing reads with Cutadapt version 1.3 (64) and then aligned to the mouse genome (mm10) with Bowtie2 version 2.1.0 with the parameter –X 2,000. PCR duplicates were removed with Picard's markDuplicates version 2.17.8, and aligned reads were sorted and filtered with SAMtools version 1.4.1. For the visualization of fragment coverage, TDFs were generated with IGVTools version 2.3.31.

Peak Calling. Aligned ATAC-seq reads were trimmed to 29 bases closest to the Tn5 cut site with bedtools version 2.26.0 (65), and then, peaks were called with MACS2 version 2.1.1 (66) using parameters—bw 29—nomodel –q 0.0001. Summits of called peaks across all samples were merged and "slopped" ±100 bp to create a master peak reference file using bedtools version 2.26.0. Peaks were annotated with the names of closest genes using a mouse OT-I TSS BED file and bedtools version 2.26.0 (closest –D ref –t all). Peaks with summits within 500 bp from TSSs were labeled promoter peaks and summits further than 500 bp were labeled enhancer peaks. Peak coverage for each ATAC-seq sample was calculated using bedtools version 2.26.0 (intersect; coverage).

ATAC Peak Analysis. Calculated peak coverage values for two ATAC-seq replicate experiments were used as input for differential analysis using DESeq2 version 1.26.0. Peaks were filtered to those significantly differential ($|Log2FC| \geq 1$, p-adj $< = 0.01$), compared with unstimulated controls, and were clustered using hierarchical and *k*-means clustering methods within R. Heatmaps were generated with ComplexHeatmap. The amount of overlap of ATAC cluster peaks with published NFAT1 (Gene Expression Omnibus [GEO]: GSE64407) (40) and NF-κB p65 (GEO: GSE82078) (67) ChIP-seq datasets

were calculated with bedtools (bedtools intersect), and significant enrichment was estimated with Fisher's exact test (fisher.test within R). To do this, published NFAT ChIP-seq data originally aligned to the mouse mm9 genome assembly were first lifted to mm10 using the University of California Santa Cruz LiftOver tool (http://genome.ucsc.edu) (68). Then peaks were called on NFAT and p65 ChIP-seq data with MACS2 bdgpeakcall. Each cluster of annotated, differentially accessible peak regions was tested for de novo motif enrichment using HOMER version 4.10.3 (findMotifsGenome.pl –size 200) (39). For each HOMER test, peaks in all other clusters were used as background.

Genomic Visualizations. Genomic tracks were created by plotting BigWig files with help of Gviz (69) PMA and ionomycin ATAC-seq tracks and NF-κB ChIP-seq tracks were extracted from publicly available sources (67, 70).

Data Availability. Raw RNA-seq data, processed RNA-seq reads, raw ATAC-seq data, and processed ATAC-seq reads generated in this study have been deposited in the Gene Expression Omnibus and the Sequence Read Archive (GSE167304). Publicly available datasets were used for this work (GSE64407; GSE82078; and GSE64409).

ACKNOWLEDGMENTS. We thank Regina Whitehead, Sharlene Hubbard, and Loni Perrenoud for their technical assistance. We thank members of the A.R. laboratory and Joonsoo Kang's laboratory for the sharing of laboratory space. We thank Principia Biopharma for providing PRN694. We thank the Department of Animal Medicine at the University of Massachusetts Medical School and University of Colorado Anschutz for maintaining our mouse colony. This work was supported by NIH National Institute of Allergy and Infectious Diseases Grants AI132419 and AI043976 (to L.J.B.).

1. S. E. Henrickson *et al*., T cell sensing of antigen dose governs interactive behavior with dendritic cells and sets a threshold for T cell activation. *Nat. Immunol.* **9**, 282–291 (2008).
2. D. Zehn, S. Y. Lee, M. J. Bevan, Complete but curtailed T-cell response to very low-affinity antigen. *Nature* **458**, 211–214 (2009).
3. N. Zhang, M. J. Bevan, CD8(+) T cells: Foot soldiers of the immune system. *Immunity* **35**, 161–168 (2011).
4. K. Tkach, G. Altan-Bonnet, T cell responses to antigen: Hasty proposals resolved through long engagements. *Curr. Opin. Immunol.* **25**, 120–125 (2013).
5. C. Rosette *et al*., The impact of duration versus extent of TCR occupancy on T cell activation: A revision of the kinetic proofreading model. *Immunity* **15**, 59–70 (2001).
6. A. K. Chakraborty, A. Weiss, Insights into the initiation of TCR signaling. *Nat. Immunol.* **15**, 798–807 (2014).
7. M. Podtschaske *et al*., Digital NFATc2 activation per cell transforms graded T cell receptor activation into an all-or-none IL-2 expression. *PLoS One* **2**, e935 (2007).
8. M. R. Müller, A. Rao, NFAT, immunity and cancer: A transcription factor comes of age. *Nat. Rev. Immunol.* **10**, 645–656 (2010).
9. B. Dura *et al*., Profiling lymphocyte interactions at the single-cell level by microfluidic cell pairing. *Nat. Commun.* **6**, 5940 (2015).
10. M. P. Gallagher, J. M. Conley, L. J. Berg, Peptide antigen concentration modulates digital NFAT1 activation in primary mouse naive CD8 $^+$ T cells as measured by flow cytometry of isolated cell nuclei. *Immunohorizons* **2**, 208–215 (2018).
11. G. Altan-Bonnet, R. N. Germain, Modeling T cell antigen discrimination based on feedback control of digital ERK responses. *PLoS Biol.* **3**, e356 (2005).
12. J. Das *et al*., Digital signaling and hysteresis characterize Ras activation in lymphoid cells. *Cell* **136**, 337–351 (2009).
13. L. M. Kingeter, S. Paul, S. K. Maynard, N. G. Cartwright, B. C. Schaefer, Cutting edge: TCR ligation triggers digital activation of NF-κB. *J. Immunol.* **185**, 4520–4524 (2010).
14. R. E. Dolmetsch, R. S. Lewis, C. C. Goodnow, J. I. Healy, Differential activation of transcription factors induced by Ca2+ response amplitude and duration. *Nature* **386**, 855–858 (1997). Correction in: *Nature* **388**, 308 (1997).
15. R. Nayar *et al*., TCR signaling via Tec kinase ITK and interferon regulatory factor 4 (IRF4) regulates CD8+ T-cell differentiation. *Proc. Natl. Acad. Sci. U.S.A.* **109**, E2794–E2802 (2012).
16. J. M. Conley, M. P. Gallagher, A. Rao, L. J. Berg, Activation of the Tec kinase ITK controls graded IRF4 expression in response to variations in TCR signal strength. *J. Immunol.* **205**, 335–345 (2020).
17. A. H. Andreotti, P. L. Schwartzberg, R. E. Joseph, L. J. Berg, T-cell signaling regulated by the Tec family kinase, Itk. *Cold Spring Harb. Perspect. Biol.* **2**, a002287 (2010).
18. J. M. Conley, M. P. Gallagher, L. J. Berg, T cells and gene regulation: The switching on and turning up of genes after T cell receptor stimulation in CD8 T cells. *Front. Immunol.* **7**, 76 (2016).
19. K.-Q. Liu, S. C. Bunnell, C. B. Gurniak, L. J. Berg, T cell receptor-initiated calcium release is uncoupled from capacitative calcium entry in Itk-deficient T cells. *J. Exp. Med.* **187**, 1721–1727 (1998).
20. A. T. Miller, H. M. Wilcox, Z. Lai, L. J. Berg, Signaling through Itk promotes T helper 2 differentiation via negative regulation of T-bet. *Immunity* **21**, 67–80 (2004).
21. L. O. Atherly, M. A. Brehm, R. M. Welsh, L. J. Berg, Tec kinases Itk and Rlk are required for CD8$^+$ T cell responses to virus infection independent of their role in CD4$^+$ T cell help. *J. Immunol.* **176**, 1571–1581 (2006).
22. C. Broussard *et al*., Altered development of CD8+ T cell lineages in mice deficient for the Tec kinases Itk and Rlk. *Immunity* **25**, 93–104 (2006).
23. R. Balyan *et al*., Modulation of naive CD8 T cell response features by ligand density, affinity, and continued signaling via internalized TCRs. *J. Immunol.* **198**, 1823–1837 (2017).
24. A. C. Richard *et al*., T cell cytolytic capacity is independent of initial stimulation strength. *Nat. Immunol.* **19**, 849–858 (2018).
25. Y. Zhong *et al*., Targeting interleukin-2-inducible T-cell kinase (ITK) and resting lymphocyte kinase (RLK) using a novel covalent inhibitor PRN694. *J. Biol. Chem.* **290**, 5960–5978 (2015).
26. L. J. Berg, L. D. Finkelstein, J. A. Lucas, P. L. Schwartzberg, Tec family kinases in T lymphocyte development and function. *Annu. Rev. Immunol.* **23**, 549–600 (2005).
27. J. E. Smith-Garvin, G. A. Koretzky, M. S. Jordan, T cell activation. *Annu. Rev. Immunol.* **27**, 591–619 (2009).
28. R. J. Brownlie, R. Zamoyska, T cell receptor signalling networks: Branched, diversified and bounded. *Nat. Rev. Immunol.* **13**, 257–269 (2013).
29. F. Marangoni *et al*., The transcription factor NFAT exhibits signal memory during serial T cell interactions with antigen-presenting cells. *Immunity* **38**, 237–249 (2013).
30. P. C. Lucas, L. M. McAllister-Lucas, G. Nunez, NF-kappaB signaling in lymphocytes: A new cast of characters. *J. Cell Sci.* **117**, 31–39 (2004).
31. K. Ishiguro *et al*., Ca2+/calmodulin-dependent protein kinase II is a modulator of CARMA1-mediated NF-kappaB activation. *Mol. Cell. Biol.* **26**, 5497–5508 (2006).
32. K. S. Ullman, J. P. Northrop, C. L. Verweij, G. R. Crabtree, Transmission of signals from the T lymphocyte antigen receptor to the genes responsible for cell proliferation and immune function: The missing link. *Annu. Rev. Immunol.* **8**, 421–452 (1990).
33. J. Jain, C. Loh, A. Rao, Transcriptional regulation of the IL-2 gene. *Curr. Opin. Immunol.* **7**, 333–342 (1995).
34. J. W. Tullai *et al*., Immediate-early and delayed primary response genes are distinct in function and genomic architecture. *J. Biol. Chem.* **282**, 23981–23995 (2007).
35. K. Man *et al*., The transcription factor IRF4 is essential for TCR affinity-mediated metabolic programming and clonal expansion of T cells. *Nat. Immunol.* **14**, 1155–1165 (2013).
36. M. Huber, M. Lohoff, IRF4 at the crossroads of effector T-cell fate decision. *Eur. J. Immunol.* **44**, 1886–1895 (2014).
37. R. Nayar *et al*., Graded levels of IRF4 regulate CD8$^+$ T cell differentiation and expansion, but not attrition, in response to acute virus infection. *J. Immunol.* **192**, 5881–5893 (2014).
38. J. D. Buenrostro, P. G. Giresi, L. C. Zaba, H. Y. Chang, W. J. Greenleaf, Transposition of native chromatin for fast and sensitive epigenomic profiling of open chromatin, DNA-binding proteins and nucleosome position. *Nat. Methods* **10**, 1213–1218 (2013).
39. S. Heinz *et al*., Simple combinations of lineage-determining transcription factors prime cis-regulatory elements required for macrophage and B cell identities. *Mol. Cell* **38**, 576–589 (2010).
40. G. J. Martinez *et al*., The transcription factor NFAT promotes exhaustion of activated CD8$^+$ T cells. *Immunity* **42**, 265–278 (2015).
41. N. P. Shinners *et al*., Bruton's tyrosine kinase mediates NF-κ B activation and B cell survival by B cell-activating factor receptor of the TNF-R family. *J. Immunol.* **179**, 3872–3880 (2007).
42. J. B. Petro, S. M. Rahman, D. W. Ballard, W. N. Khan, Bruton's tyrosine kinase is required for activation of IkappaB kinase and nuclear factor kappaB in response to B cell receptor engagement. *J. Exp. Med.* **191**, 1745–1754 (2000).
43. P. Antony *et al*., B cell receptor directs the activation of NFAT and NF-kappaB via distinct molecular mechanisms. *Exp. Cell Res.* **291**, 11–24 (2003).
44. G. Gaud, R. Lesourne, P. E. Love, Regulatory mechanisms in T cell receptor signalling. *Nat. Rev. Immunol.* **18**, 485–497 (2018).
45. L. Chen, D. B. Flies, Molecular mechanisms of T cell co-stimulation and co-inhibition. *Nat. Rev. Immunol.* **13**, 227–242 (2013).
46. J. Cheng, A. Montecalvo, L. P. Kane, Regulation of NF-κB induction by TCR/CD28. *Immunol. Res.* **50**, 113–117 (2011).
47. R. Brignall *et al*., Integration of kinase and calcium signaling at the level of chromatin underlies inducible gene activation in T cells. *J. Immunol.* **199**, 2652–2667 (2017).
48. M. Trebak, J.-P. Kinet, Calcium signalling in T cells. *Nat. Rev. Immunol.* **19**, 154–169 (2019).
49. S. Heinzel *et al*., A Myc-dependent division timer complements a cell-death timer to regulate T cell and B cell responses. *Nat. Immunol.* **18**, 96–103 (2017).
50. B. B. Au-Yeung *et al*., IL-2 modulates the TCR signaling threshold for CD8 but not CD4 T cell proliferation on a single-cell level. *J. Immunol.* **198**, 2445–2456 (2017).
51. T. R. Mempel, S. E. Henrickson, U. H. Von Andrian, T-cell priming by dendritic cells in lymph nodes occurs in three distinct phases. *Nature* **427**, 154–159 (2004).
52. C. E. Clark, M. Hasan, P. Bousso, A role for the immediate early gene product c-fos in imprinting T cells with short-term memory for signal summation. *PLoS One* **6**, e18916 (2011).
53. J. Chen *et al*., NR4A transcription factors limit CAR T cell function in solid tumours. *Nature* **567**, 530–534 (2019).
54. X. Liu *et al*., Genome-wide analysis identifies NR4A1 as a key mediator of T cell dysfunction. *Nature* **567**, 525–529 (2019).
55. D. Ramsköld *et al*., Full-length mRNA-Seq from single-cell levels of RNA and individual circulating tumor cells. *Nat. Biotechnol.* **30**, 777–782 (2012). Correction in: *Nat. Biotechnol.* **38**, 374 (2020).
56. B. A. Kriegsman *et al*., Frequent loss of IRF2 in cancers leads to immune evasion through decreased MHC class I antigen presentation and increased PD-L1 expression. *J. Immunol.* **203**, 1999–2010 (2019).
57. A. M. Bolger, M. Lohse, B. Usadel, Trimmomatic: A flexible trimmer for Illumina sequence data. *Bioinformatics* **30**, 2114–2120 (2014).
58. B. Langmead, S. L. Salzberg, Fast gapped-read alignment with Bowtie 2. *Nat. Methods* **9**, 357–359 (2012).

59. B. Li, C. N. Dewey, RSEM: Accurate transcript quantification from RNA-seq data with or without a reference genome. *BMC Bioinformatics* **12**, 323 (2011).
60. M. E. Ritchie *et al*., limma powers differential expression analyses for RNA-sequencing and microarray studies. *Nucleic Acids Res.* **43**, e47 (2015).
61. M. I. Love, W. Huber, S. Anders, Moderated estimation of fold change and dispersion for RNA-seq data with DESeq2. *Genome Biol.* **15**, 550 (2014).
62. Z. Gu, R. Eils, M. Schlesner, Complex heatmaps reveal patterns and correlations in multidimensional genomic data. *Bioinformatics* **32**, 2847–2849 (2016).
63. G. Yu, L.-G. Wang, Y. Han, Q.-Y. He, clusterProfiler: An R package for comparing biological themes among gene clusters. *OMICS* **16**, 284–287 (2012).
64. M. Martin, Cutadapt removes adapter sequences from high-throughput sequencing reads. *EMBnet. J.* **17**, 10–12 (2011).
65. A. R. Quinlan, I. M. Hall, BEDTools: A flexible suite of utilities for comparing genomic features. *Bioinformatics* **26**, 841–842 (2010).
66. Y. Zhang *et al*., Model-based analysis of ChIP-Seq (MACS). *Genome Biol.* **9**, R137 (2008).
67. H. Oh *et al*., An NF-κB transcription-factor-dependent lineage-specific transcriptional program promotes regulatory T cell identity and function. *Immunity* **47**, 450–465.e5 (2017).
68. A. S. Hinrichs *et al*., The UCSC Genome Browser Database: Update 2006. *Nucleic Acids Res.* **34**, D590–D598 (2006).
69. F. Hahne, R. Ivanek, Visualizing genomic data using Gviz and Bioconductor. *Methods Mol. Biol.* **1418**, 335–351 (2016).
70. G. P. Mognol *et al*., Exhaustion-associated regulatory regions in $CD8^+$ tumor-infiltrating T cells. *Proc. Natl. Acad. Sci. U.S.A.* **114**, E2776–E2785 (2017).